Journal of Applied Electrochemistry (2018) 48:487–494
https://doi.org/10.1007/s10800-018-1181-7

RESEARCH ARTICLE

Ionic liquid treated carbon nanotube sponge as high areal capacity cathode for lithium sulfur batteries

Henry Taisun Lin[1] · Gang Yang[2] · Yi-Yun Timothy Tsao[3] · Yifan Liu[1] · Choongho Yu[1,2]

Received: 10 August 2017 / Accepted: 5 March 2018 / Published online: 10 March 2018

Abstract

Ionic liquid (1-ethyl-3-methylimidazolium tetrafluoroborate) treated carbon nanotube (CNT) sponges were tested as a conductive matrix and polysulfide reservoir for the cathode of lithium–sulfur batteries. X-ray photoelectron spectroscopy results confirmed that this treatment doped fluorine and oxygen on the surface of the CNT, and experimental results showed that this treatment had significantly improved adsorption of polysulfides in the CNT sponge. As a result, this sponge cathode accommodated a remarkably high sulfur areal loading of 8 mg cm^{-2}, showing a high areal capacity of 7.1 mAh cm^{-2} at the 100th cycle at an areal current density of 1.28 mA cm^{-2} with an average capacity fading of 0.048% per cycle. The adsorbing energy of Li_2S_6 on the F/O-doped carbon structure was calculated using the density functional theory, confirming that the doping made the polysulfide adsorption stable particularly due to fluorine. This study provides a useful approach of simultaneously introducing both fluorine and oxygen to carbon in order to significantly improve the polysulfide adsorption on the carbon cathode and thereby obtain high areal discharge capacity, which is much more important than specific discharge capacity for actual battery operation.

Graphical Abstract

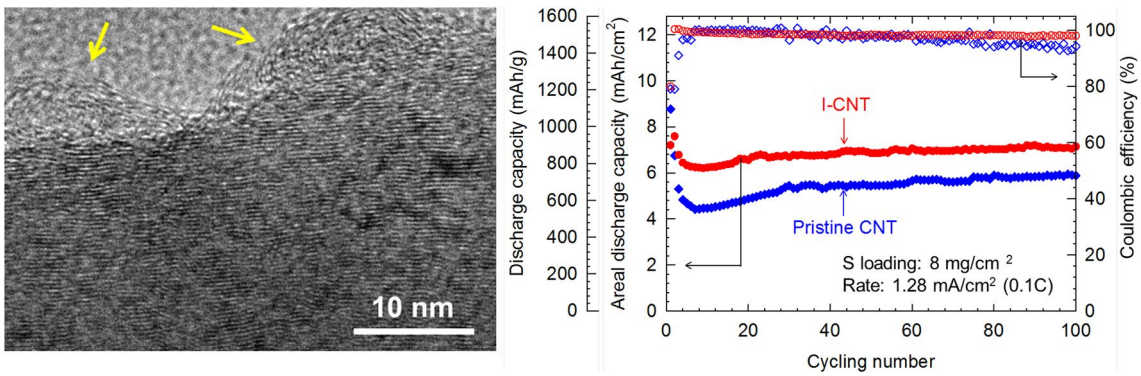

Keywords Carbon nanotube · Ionic liquid · Areal capacity · CNT sponge · High sulfur loading

✉ Choongho Yu
chyu@tamu.edu

[1] Department of Materials Science and Engineering, Texas A&M University, College Station, TX 77843, USA

[2] Department of Mechanical Engineering, Texas A&M University, College Station, TX 77843, USA

[3] Department of Chemistry, Texas A&M University, College Station, TX 77843, USA

Lithium–sulfur (Li–S) batteries are attractive candidates to meet the requirements for the next-generation energy storage because of the higher theoretical energy density (2600 Wh kg^{-1}) and capacity (1673 mAh g^{-1}) of sulfur compared to popular Li-ion batteries [1–10]. For practical use, however, it is necessary to address the key problems in Li–S batteries such as a large amount of inactive binders and conductive additives in cathode, low utilization of sulfur particularly for the case with a high sulfur loading,

and polysulfide shuttle [5, 11, 12], which make the current Li–S batteries similar or inferior to the current Li-ion batteries [13]. Over the past years, various brilliant ideas have been rigorously suggested to alleviate the polysulfide shuttle problems, significantly extending cycling performance [3, 5–8]. Now it is time to study how to increase the sulfur loading rather than specific capacity based on sulfur because the sulfur loading is closely tied to the actual amount of energy stored in batteries.

In typical Li–S batteries, insulating sulfur and polysulfides necessitate conductive additives such as carbon black [1, 14], graphene [15, 16], and carbon nanotube (CNT) [5, 16] in cathode. The additives and sulfur are powdery, which requires a binder to make a cathode but the binder is insulating and inactive, which increases the weight and the cost of the cathode. Moreover, the intermediate polysulfides are in liquid phase during charge/discharge processes, and they may smear out from cathode, demanding more conducting additives to maintain the battery performance. These inactive materials lessen the relative amount of sulfur in cathode, eventually resulting in only a moderate energy density in actual battery cells due to a low sulfur loading. Therefore, it is important to find an effective method for increasing the areal sulfur loading in the cathode of Li-S batteries.

A large surface area and a high affinity to polysulfides are other crucial features of the cathode of Li-S batteries. When the sulfur loading in cathode is too high, the liquid-phase polysulfides can easily migrate to anode irreversibly. This not only reduces the active sulfur in cathode, but also degrades the performance due to the passivation of anode surface. To have a high-affinity surface, it has been found that surface modifications with functional groups and nanoparticles on carbonaceous cathode materials are effective [3, 6–9].

Here, we have alleviated the aforementioned two problems encountered with a high sulfur loading by eliminating the inactive binder and enlarging the cathode surface area with an increased polysulfide affinity. Our Li–S batteries employ three-dimensional (3-D) sponge-like CNT bulks whose CNTs are connected during the synthesis process. The synthesis process of this binder-free CNT sponge is suitable for mass production with low cost [17, 18]. The CNT has many walls and some of the outer walls have been exfoliated using a simple treatment with an ionic liquid (1-ethyl-3-methylimidazolium tetrafluoroborate, [EMIM][BF_4]). This treatment also promotes chemisorption of polysulfides on the CNT due to the modification of the graphitic carbon with polysulfide-attracting groups [19–21].

The CNT sponge was synthesized by a chemical vapor deposition (CVD) method using ethylene gas (Airgas, 99.999%) and ferrocene (Sigma Aldrich, 98%) as a carbon source and a catalyst, respectively [22]. A cylindrical CNT sponge (Fig. 1a) was synthesized in a 22-mm inner diameter quartz tube, which was placed inside a three-zone tube furnace (Lindberg/Blue M STF55346C). Prior to the synthesis process, the ferrocene catalyst powders were placed in zone 1 (upstream) and then Ar (Airgas, 99.999%) was passed through the tube with a flow rate of 200 sccm for 10 min to purge air in the tube. Afterwards, the Ar gas was switched to H_2 with a flow rate of 260 sccm. At the same time, the temperatures of zone 1 and zone 3 were raised to 120 °C within 20 min and 650 °C within 10 min, respectively. After the targeted temperatures were reached, 80 sccm Ar gas passing through a water bubbler and 80 sccm C_2H_4 (Airgas, 99.999%) were added to the gas flow for 0.5–1 h to grow cylindrical sponge-like CNTs from the inner wall of the tube. Then the furnace was cooled down with 200-sccm Ar gas.

The as-synthesized CNT sponge was immersed in the ionic liquid, [EMIM][BF_4] (Sigma Aldrich, 99%), and then heated to 200 °C within 20 min. The temperature of the sample was maintained at 200 °C for 1 h, and then the sample was naturally cooled down to room temperature. This treatment process was carried out in an ambient condition to get oxygen exposure. The CNT sponge was immersed into deionized water at ~ 70 °C overnight for several times to get rid of ionic liquid residues. Finally, the CNT sponge was dried in a vacuum oven at ~ 60 °C.

The morphology was inspected by an FEI Quanta 600 scanning electron microscope (SEM) and a JEOL JEM-2010 transmission electron microscope (TEM). The pristine CNT sponge consists of many entangled and connected CNTs [17, 22, 23]. After the ionic liquid treatment, the structural integrity of the CNT sponge (I-CNT) was maintained (Fig. 1b), but the outer walls (graphitic layers) of the CNT were exfoliated and etched (Fig. 1c). High-resolution TEM images display wavy graphitic layers (Fig. 1d) and graphitic layers disengaged from the CNT (Fig. 1e).

X-ray photoelectron spectra (XPS) were obtained using an Omicron XPS/UPS system with Argus detector using Mg Kα as X-ray source to investigate the surface chemical compositions of the I-CNT and the pristine CNT (Fig. 2a). The XPS peak near 688 eV from I-CNT was identified as C–F bonds (Fig. 2b), which could be resulted from BF_4^- in the ionic liquid [24]. This peak would be composed of three different C–F bonds—sp^2 C–F (semi-ionic) bond, chemical (covalent) bond, and C–F physical bond [24]. We also noticed that the peak corresponding to O 1s near 532 eV became prominent after the ionic liquid treatment, which could be ascribed to oxygen exposure from ambient air during the treatment process. The relative amounts of oxygen and fluorine in the pristine CNT and the I-CNT are displayed in Table 1 by normalizing at% of oxygen and fluorine by the at% of carbon.

These additional elements could play an important role in attracting polysulfides to alleviate the polysulfide shuttle

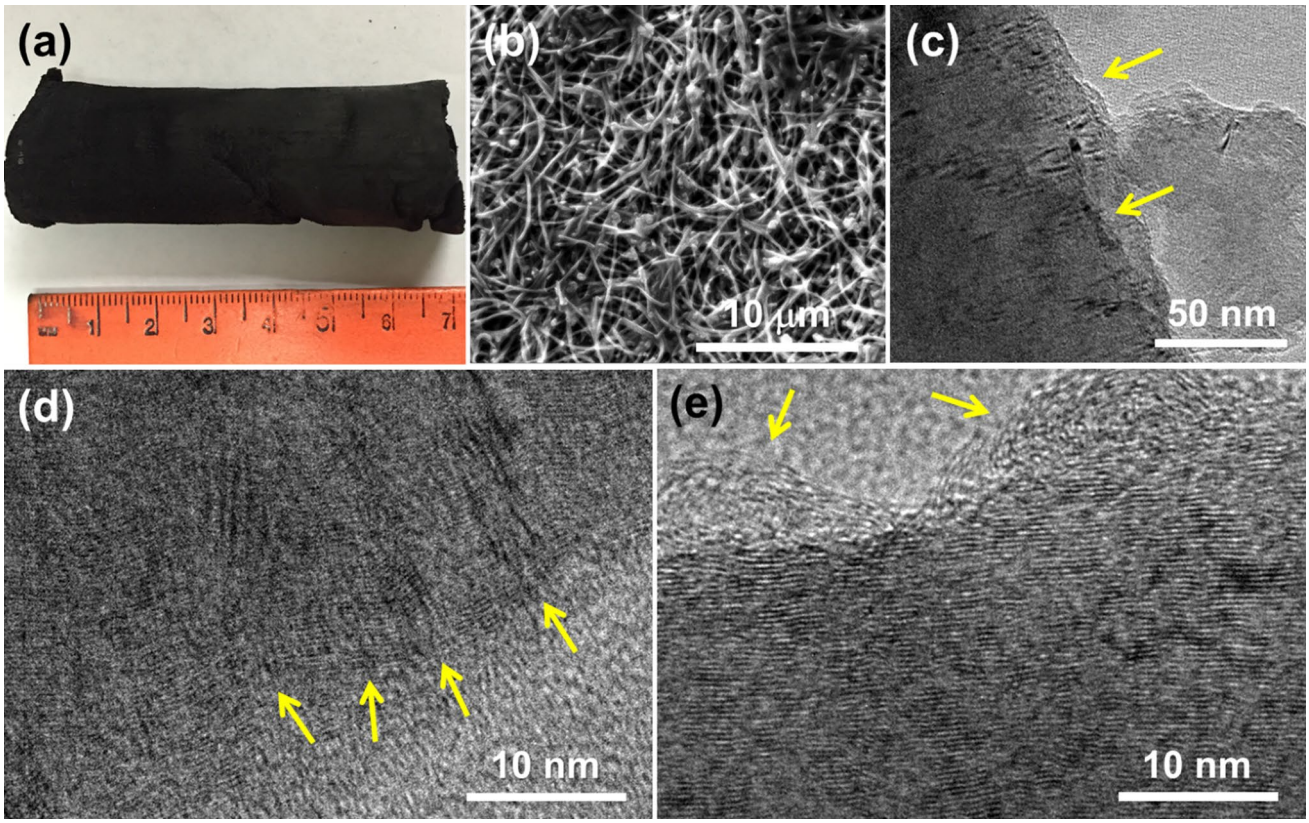

Fig. 1 **a** A photograph of an as-synthesized CNT sponge. SEM (**b**) and TEM (**c**–**e**) images of I-CNT (CNT after the ionic liquid treatment). The TEM images show etched surfaces (**c**), wavy graphitic layers (**d**), and disengaged graphitic layers (**e**)

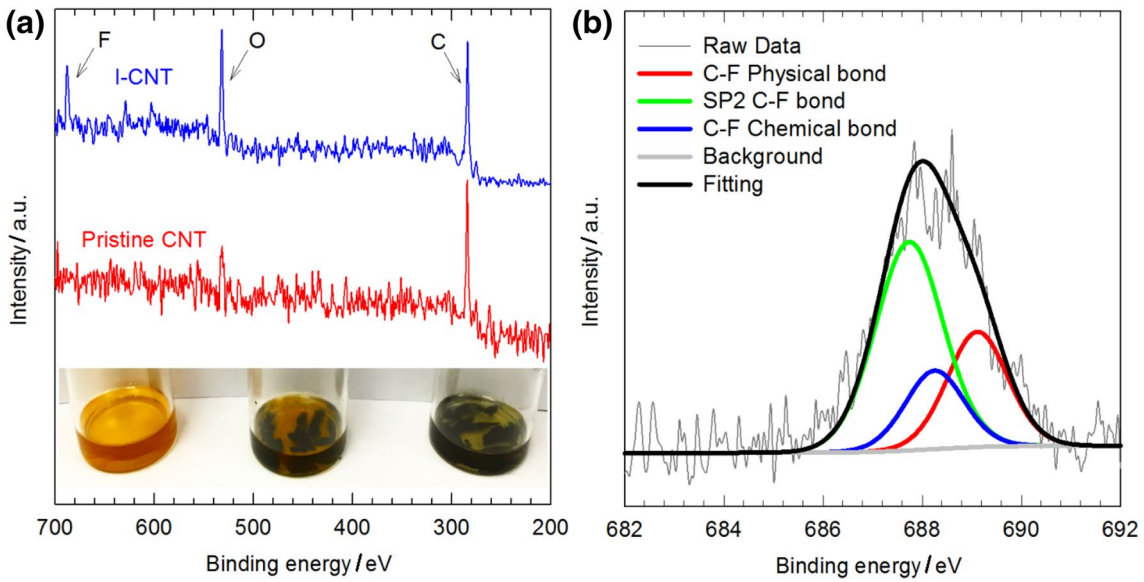

Fig. 2 **a** XPS scan results of the I-CNT and the pristine CNT, showing prominent F and O peaks after the ionic liquid treatment. The inset shows photographs of a pristine Li_2S_6 solution (left), a Li_2S_6 solution with pristine CNT sponges (middle), and a Li_2S_6 solution with I-CNT sponges (right). **b** XPS analysis results of the I-CNT corresponding to F 1s. (Color figure online)

Table 1 Element content (at%) of the pristine CNT and I-CNT normalized by at% of carbon based on the XPS results

Element	O (at%)/C(at%)	F (at%)/C(at%)
CNT	17.3%	–
I-CNT	30.0%	9.0%

problem. To qualitatively test the affinity of polysulfides to I-CNT, pristine CNT and I-CNT sponges were separately immersed into an 1 mM Li_2S_6 solution (molar concentration based on S atom). To prepare the solution, sulfur (Sigma Aldrich, 99.5%) and Li_2S (Sigma Aldrich, 99.98%) were dissolved in 1,3-dioxolane:1,2-dimethoxyethane (DOL:DME) (1:1 by volume, Alfa Aesar, 99%) in a 5:1 molar ratio, and then the mixture was stirred and heated at 90 °C for 3 days in an Ar atmosphere until a reddish solution was formed, as shown in the left vial of the inset of Fig. 2a. When 3.6 mg of pristine CNT sponges was immersed in a 2 mL polysulfide solution, the color of the solution was barely changed (the middle vial). However, after adding 3.6 mg I-CNT sponge to the solution, the reddish color disappeared (the right vial), suggesting polysulfides were adsorbed on I-CNT.

The influence of I-CNT sponge on the battery cell performance was then identified when it was used as the cathode of Li–S batteries. First, the CNT sponges were sliced and cut into a coin shape (~ 3/8 inch in diameter) with a thickness of ~ 1 mm to make coin cells. A desired amount of sulfur powders were spread over one coin-shaped sponge, and then another one was placed on top of the sulfur. Subsequently, the sulfur-sandwiched CNT sponge was cold-pressed by applying 2 ton force for 10 min to have a compact cathode, whose thickness became ~ 0.2 mm. To assemble CR2032 type coin cells, a Li metal foil and a Celgard 2400 separator were stacked, and ~ 10 µL of electrolyte [1-M lithium bis(trifluoromethanesulfonyl)imide (LiTFSI) and 0.5 M $LiNO_3$ dissolved in DOL:DME (1:1 v/v)] were subsequently applied. Afterwards, the cathode was placed onto the separator, followed by adding 80 µL of the electrolyte. The cells were cycled between 1.7 and 3 V at desired rates (1C = 1600 mA g^{-1}) using an Arbin BT2000 battery tester.

Figure 3a shows the cycling performances of the cells made of the pristine CNT and the I-CNT with an areal current density of 1.20 mA cm^{-2}, which corresponds to 0.25 C (1 C = 1600 mA g^{-1}) when the areal loading of sulfur is 3 mg cm^{-2} (CNT:S = 8:3 weight ratio). The specific discharge capacity of the cell made of the pristine CNT was only 617 mAh g^{-1} (based on sulfur) after 100 cycles. In contrast, the specific discharge capacity of the cell made of the I-CNT sponge (I-CNT cell) was much higher after 100 cycles (1121 mAh g^{-1}). Except the capacity fading at the initial several activation cycles [11, 12], the capacity of the I-CNT cell was stably maintained. For instance, the specific capacities of the I-CNT cell at the 3rd and 100th cycles were 1174 and 1121 mAh g^{-1}, respectively, which shows 95% capacity retention. The average capacity fading rate was 0.048% per cycle and the Coulombic efficiency of each cycle was higher than 98%, which confirms that the I-CNT can effectively hold polysulfides in cathode, as demonstrated in the inset of Fig. 2a, and thus the polysulfide shuttle could be suppressed. Furthermore, the areal discharge capacity was relatively large, showing 3.4 mAh cm^{-2} at the 100th cycle.

The "areal" discharge capacity is a much more important parameter to evaluate the actual cell performance rather than the "specific" discharge capacity. It should be noted that the specific discharge capacity indicates the degree of sulfur utilization. As the sulfur loading gets lower, more sulfur participates in charge/discharge reactions, resulting in a higher specific capacity. However, when it comes to the actual cell performance, besides the degree of sulfur utilization, the total sulfur loading should be considered. Therefore, it may be misleading for the cell performance if only showing the specific capacity.

When the sulfur loading was significantly increased to a higher level, 8 mg cm^{-2} (CNT:S = 5:5 weight ratio), while maintaining the areal current density at a similar level, 1.28 mA cm^{-2} (0.1 C), the areal discharge capacity was remarkably increased to 7.1 mAh cm^{-2} at the 100th cycle (Fig. 3b), which is higher than the values in many previously published literature [4, 12, 20, 25–30] and comparable to the values in very recent literature [31–34]. It should be noted that the larger areal capacity with the higher sulfur loading reduced the specific capacity of the I-CNT cell (i.e., less sulfur utilization due to the higher sulfur loading), but the capacity still remained to be 880 mAh g^{-1} after 100 cycles. The capacity of the higher sulfur loading cases (i.e. 8 mg cm^{-2}) was continuously increased, which indicates that sulfur was less utilized at the beginning due to inhomogeneously distributed sulfur [18]. While the specific discharge capacity of the pristine CNT cell was similar in the range of 600–700 mAh g^{-1} for both sulfur loading cases, that of the I-CNT cell was reduced with the higher sulfur loading. Although the sulfur is less utilized for the higher sulfur loading case, it is useful to increase the sulfur loading in order to enlarge the actual energy density.

Figure 4 shows discharge/charge curves of the I-CNT and pristine CNT cells. The I-CNT cell shows more stable discharge/charge curves from the 3rd cycle while the pristine CNT cell exhibited continuous changes in the curves. The average capacity fading rates of the I-CNT and pristine CNT cells were, respectively, 0.47 and 3.0% per cycle when comparing their 3rd and 100th cycles. Here the first two cycles were not used for the comparison since cells need at least a few cycles to reach a relatively stable or equilibrium state. The I-CNT cell shows slightly lower discharge potentials

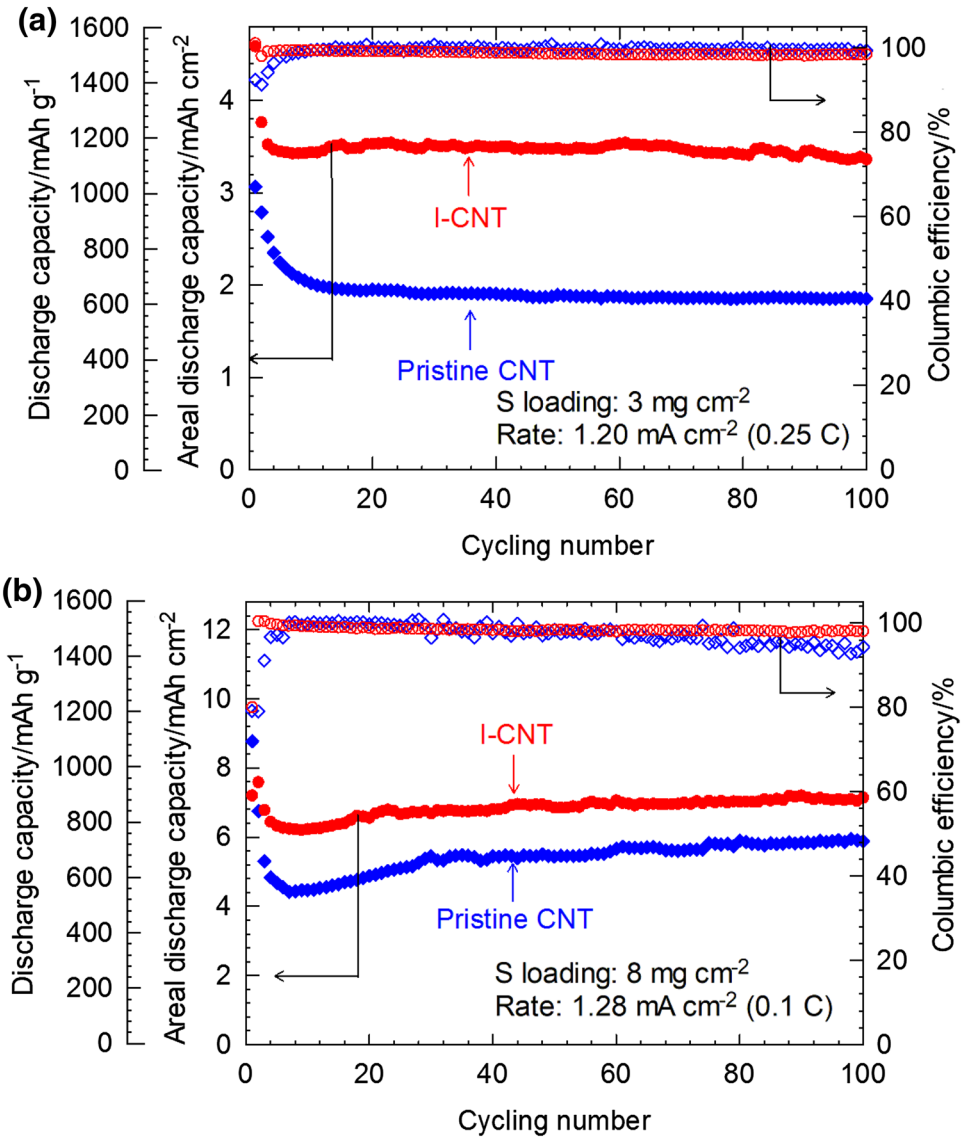

Fig. 3 Cycling performances and Coulombic efficiencies of the cells made of I-CNT and pristine CNT cathodes when **a** sulfur areal loading was 3 mg cm^{-2} and discharge/charge rate was 1.20 mA cm^{-2} (0.25 C) and **b** sulfur areal loading was 8 mg cm^{-2} and discharge/charge rate was 1.28 mA cm^{-2} (0.1 C). The discharge capacity was obtained based on sulfur

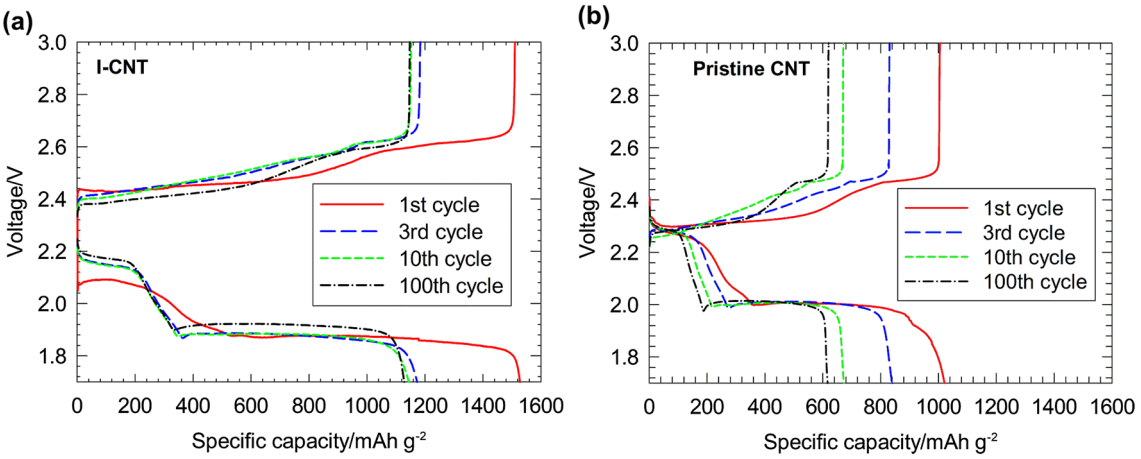

Fig. 4 Discharge and charge curves at 1st, 3rd, 10th, and 100th cycles when the I-CNT (**a**) or the pristine CNT (**b**) was used. Sulfur loading was 3 mg cm^{-2} and discharge/charge rate was 1.20 mA cm^{-2} (0.25 C). (Color figure online)

presumably due to larger overpotentials caused by the more resistive exfoliated outer layers of the CNT compared to those of the pristine CNT.

While the outstanding performance of our cells partly comes from the binder-free structure and excellent electrical conductivity of interconnected CNTs in the CNT sponge cathode, the functional groups on the CNT surface would also play a crucial role due to the higher sulfur utilization (i.e., reducing dead sulfur) and the lower sulfur loss to anode (i.e., reducing polysulfide shuttle). To further investigate their roles, the most stable conformers were identified using density function theory (DFT) calculations. In particular, the sulfur adsorption on fluorine-containing carbon was seldom mentioned unlike the previously studied polysulfide immobilization effect with O and N doping on carbon [3, 20, 35–37].

Here, coronene molecule, containing 24 carbon atoms with 12 hydrogen atoms, was used to represent the carbon terminated at its edges. Li_2S_6 was chosen as a model for the polysulfides. All calculations were carried out by the first principle DFT implemented with the Gaussian 09 software package. The B3LYP/6-31 + G(d,p) level of computation was used for all structures to optimize geometries and acquire the electronic energies. The electronic energy difference between the adsorbed system and isolated system was calculated to obtain the binding energy of the sulfur adsorbed on carbonyl and fluorine sites of the model. The adsorbing energy is defined as the enthalpy change (ΔH) between separated and adsorbed states of Li_2S_6 adsorbate and different adsorbing sites.

We considered three different configurations for the carbon structure—the pristine carbon as a reference, a fluorine-doped carbon, and a both fluorine/oxygen-doped carbon because of the large amount of oxygen in I-CNT. The calculated adsorbing energy (ΔH) between Li_2S_6 and carbon for the pristine carbon (− 1.01 eV) was altered to − 1.98 eV after the fluorine doping. The calculated ΔH values are displayed in Table 2 and their optimized structures are shown in Fig. 5. Here, the more negative ΔH of the fluorine-doped carbon suggests that the fluorine doping makes the adsorption more thermodynamically stable. The lone pair electrons of fluorine could form a Lewis acid–base pair with Li_2S_x, and thereby polysulfides could be effectively attracted near the fluorine. The greater electronegativity difference between fluorine and carbon atoms compared to that between carbon atoms would cause highly polar C–F bonds, which results in a stronger Coulombic interaction between the positively and negatively charged atoms. As a result, we suggest a reasonable hypothesis that lithium tends to approach fluorine in

Table 2 DFT calculation results of the adsorbing energy (ΔH) between different adsorption sites and adsorbed Li_2S_6

Doping	None (Pristine)	F only	F and –COOH		–COOH only
Adsorption site	–	C–F	C–F	–COOH	–COOH
ΔH (eV)	− 1.01	− 1.98	− 2.36	− 1.34	− 1.36

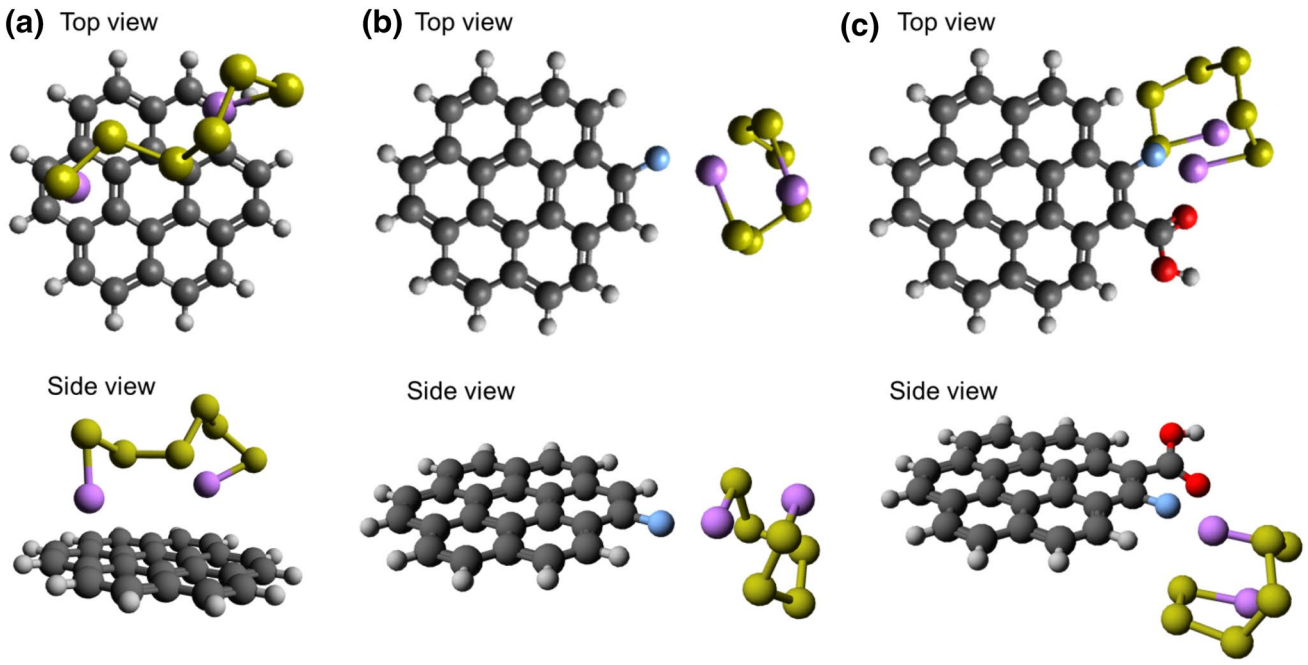

Fig. 5 Top and side views of Li_2S_6 adsorbed on **a** a pristine carbon group, **b** a fluorine-doped carbon, and **c** a fluorine-doped carbon with –COOH group. Black, gray, yellow, purple, red, and blue balls represent C, H, S, Li, O, and F atoms, respectively. (Color figure online)

order to stabilize the system by reducing the system energy. An intuitive evidence of this hypothesis is their relative positions shown in Fig. 5b, c—the Li atom in Li_2S_6 is the closest to the F atom.

When fluorine is co-doped with oxygen (Fig. 5c), ΔH between Li_2S_6 and F became more negative to − 2.36 eV compared to − 1.98 eV from that of the fluorine-doped carbon. We believe that lithium could be similarly attracted to the negatively charged oxygen in –COOH group, which has been identified to display a good polysulfide adsorbing characteristic [12, 19]. On the other hand, ΔH of Li_2S_6 adsorbed on –COOH group on the fluorine-doped carbon is − 1.34 eV, which is better than that of the pristine carbon, but worse than those of Li_2S_6 and F. In addition, ΔH of Li_2S_6 adsorbed on –COOH group on the carbon without fluorine was similar (− 1.36 eV). The computational results indicate that Li_2S_6 has stronger affinity to fluorine site compared to –COOH group, and the adsorption of the polysulfides could be further promoted by oxygen doping nearby.

In summary, we have synthesized and used porous 3-D CNT sponges as the cathode of Li–S batteries. To enhance the energy density, we attempted to treat the CNT sponge with the ionic liquid so as to increase the sulfur loading and the areal discharge capacity. This treatment created fluorine and oxygen functional groups on carbon according to XPS results, resulting in stronger polysulfide adsorbing characteristics. A high areal discharge capacity (7.1 mAh cm^{-2}) was obtained at the 100th cycle using with a high sulfur loading (8 mg cm^{-2}) and a high areal current (1.28 mA cm^{-2}), and a small average capacity fading rate of 0.048% per cycle and a high Coulombic efficiency (> 98%) were observed. Our cells also displayed decent specific discharge capacities as high as 1121 mAh g^{-1}. DFT calculation identified that the fluorine site could be attributed to the impressive performance due to the more stable adsorption of the polysulfides on the carbon structure. This work shows not only an approach of significantly improving the performance of Li–S batteries, but also identified major active sites to hold the polysulfide near cathode.

Acknowledgements The authors acknowledge financial supports from the US National Science Foundation (Award Numbers: IIP 1701200, IIP 1655429, CHE 1410272) and Texas A&M Engineering Experiment Station, and permission to use the Laboratory for Molecular Simulation at Texas A&M University, which was supported by the US National Science Foundation (Award Number: CHE 0541587).

References

1. Bauer I, Thieme S, Brückner J, Althues H, Kaskel S (2014) Reduced polysulfide shuttle in lithium–sulfur batteries using nafion-based separators. J Power Sources 251:417–422
2. Elazari R, Salitra G, Garsuch A, Panchenko A, Aurbach D (2011) Sulfur-impregnated activated carbon fiber cloth as a binder-free cathode for rechargeable Li-S batteries. Adv Mater 23:5641–5644
3. Huang J-Q, Xu Z-L, Abouali S, Garakani MA, Kim J-K (2016) Porous graphene oxide/carbon nanotube hybrid films as interlayer for lithium-sulfur batteries. Carbon 99:624–632
4. Fu Y, Su Y-S, Manthiram A (2014) Li_2S-carbon sandwiched electrodes with superior performance for lithium-sulfur batteries. Adv Energy Mater 4:1300655
5. Pu X, Yang G, Yu C (2014) Liquid-type cathode enabled by 3D sponge-like carbon nanotubes for high energy density and long cycling life of Li-S batteries. Adv Mater 26:7456–7461
6. Lu Y, Gu S, Guo J, Rui K, Chen C, Zhang S, Jin J, Yang J, Wen Z (2017) Sulfonic groups originated dual-functional interlayer for high performance lithium-sulfur battery. ACS Appl Mater Interfaces 9:14878–14888
7. Hwang J-Y, Kim HM, Lee S-K, Lee J-H, Abouimrane A, Khaleel MA, Belharouak I, Manthiram A, Sun Y-K (2016) High-energy, high-rate, lithium–sulfur batteries: synergetic effect of hollow TiO_2-webbed carbon nanotubes and a dual functional carbon-paper interlayer. Adv Energy Mater 6:1501480
8. Bhattacharya P, Nandasiri MI, Lv D, Schwarz AM, Darsell JT, Henderson WA, Tomalia DA, Liu J, Zhang J-G, Xiao J (2016) Polyamidoamine dendrimer-based binders for high-loading lithium–sulfur battery cathodes. Nano Energy 19:176–186
9. Pu X, Yu C (2012) Enhanced overcharge performance of nano-$LiCoO_2$ by novel Li_3VO_4 surface coatings. Nanoscale 4:6743–6747
10. Pu X, Yang G, Yu C (2014) Safe and reliable operation of sulfur batteries with lithiated silicon. Nano Energy 9:318–324
11. Xiao Z, Yang Z, Nie H, Lu Y, Yang K, Huang S (2014) Porous carbon nanotubes etched by water steam for high-rate large-capacity lithium–sulfur batteries. J Mater Chem A 2:8683
12. Song J, Xu T, Gordin ML, Zhu P, Lv D, Jiang Y-B, Chen Y, Duan Y, Wang D (2014) Nitrogen-doped mesoporous carbon promoted chemical adsorption of sulfur and fabrication of high-areal-capacity sulfur cathode with exceptional cycling stability for lithium-sulfur batteries. Adv Funct Mater 24:1243–1250
13. Jung YS, Cavanagh AS, Riley LA, Kang S-H, Dillon AC, Groner MD, George SM, Lee S-H (2010) Ultrathin direct atomic layer deposition on composite electrodes for highly durable and safe Li-ion batteries. Adv Mater 22:2172–2176
14. Seh ZW, Zhang Q, Li W, Zheng G, Yao H, Cui Y (2013) Stable cycling of lithium sulfide cathodes through strong affinity with a bifunctional binder. Chem Sci 4:3673
15. Sun L, Kong W, Jiang Y, Wu H, Jiang K, Wang J, Fan S (2015) Super-aligned carbon nanotube/graphene hybrid materials as a framework for sulfur cathodes in high performance lithium sulfur batteries. J Mater Chem A 3:5305–5312
16. Tang C, Zhang Q, Zhao MQ, Huang JQ, Cheng XB, Tian GL, Peng HJ, Wei F (2014) Nitrogen-doped aligned carbon nanotube/graphene sandwiches: facile catalytic growth on bifunctional natural catalysts and their applications as scaffolds for high-rate lithium-sulfur batteries. Adv Mater 26:6100–6105
17. Wang H, Tazebay AS, Yang G, Lin H, Choi W, Yu C (2016) Highly deformable thermal interface materials enabled by covalently-bonded carbon nanotubes. Carbon 106:152–157
18. Pu X, Yang G, Yu C (2015) Trapping polysulfides catholyte in carbon nanofiber sponges for improving the performances of sulfur batteries. J Electrochem Soc 162:A1396–A1400
19. Wu F, Ye Y, Chen R, Qian J, Zhao T, Li L, Li W (2015) Systematic effect for an ultralong cycle lithium-sulfur battery. Nano Lett 15:7431–7439
20. Yuan S, Bao JL, Wang L, Xia Y, Truhlar DG, Wang Y (2016) Graphene-supported nitrogen and boron rich carbon layer for improved performance of lithium-sulfur batteries due to enhanced

chemisorption of lithium polysulfides. Adv Energy Mater 6:1501733
21. Guo J, Yang Z, Yu Y, Abruna HD, Archer LA (2013) Lithium-sulfur battery cathode enabled by lithium-nitrile interaction. J Am Chem Soc 135:763–767
22 Yang G, Choi W, Pu X, Yu C (2015) Scalable synthesis of bi-functional high-performance carbon nanotube sponge catalysts and electrodes with optimum C–N–Fe coordination for oxygen reduction reaction. Energy Environ Sci 8:1799–1807
23 Erbay C, Yang G, de Figueiredo P, Sadr R, Yu C, Han A (2015) Three-dimensional porous carbon nanotube sponges for high-performance anodes of microbial fuel cells. J Power Sources 298:177–183
24 Vadahanambi S, Jung J-H, Kumar R, Kim H-J, Oh I-K (2013) An ionic liquid-assisted method for splitting carbon nanotubes to produce graphene nano-ribbons by microwave radiation. Carbon 53:391–398
25 Pang Q, Nazar LF (2016) Long-life and high-areal-capacity Li-S batteries enabled by a light-weight polar host with intrinsic polysulfide adsorption. ACS Nano 10:4111–4118
26 Song J, Yu Z, Gordin ML, Wang D (2016) Advanced sulfur cathode enabled by highly crumpled nitrogen-doped graphene sheets for high-energy-density lithium-sulfur batteries. Nano Lett 16:864–870
27 Liu S, Li Y, Hong X, Xu J, Zheng C, Xie K (2016) Reduced graphene oxide-hollow carbon sphere nanostructure cathode material with ultra-high sulfur content for high performance lithium-sulfur batteries. Electrochim Acta 188:516–522
28 Chen J, Wu D, Walter E, Engelhard M, Bhattacharya P, Pan H, Shao Y, Gao F, Xiao J, Liu J (2015) Molecular-confinement of polysulfides within mesoscale electrodes for the practical application of lithium sulfur batteries. Nano Energy 13:267–274
29 Schneider A, Weidmann C, Suchomski C, Sommer H, Janek Jr, Brezesinski T (2015) Ionic liquid-derived nitrogen-enriched carbon/sulfur composite cathodes with hierarchical microstructure-a step toward durable high-energy and high-performance lithium–sulfur batteries. Chem Mater 27:1674–1683
30 Schneider A, Suchomski C, Sommer H, Janek J, Brezesinski T (2015) Free-standing and binder-free highly N-doped carbon/sulfur cathodes with tailorable loading for high-areal-capacity lithium–sulfur batteries. J Mater Chem A 3:20482–20486
31 Chung S-H, Han P, Chang C-H, Manthiram A (2017) A shell-shaped carbon architecture with high-loading capability for lithium sulfide cathodes. Adv Energy Mater. https://doi.org/10.1002/aenm.201700537
32 Chong WG, Huang J-Q, Xu Z-L, Qin X, Wang X, Kim J-K (2017) Lithium–sulfur battery cable made from ultralight, flexible graphene/carbon nanotube/sulfur composite fibers. Adv Funct Mater 27(4):1604815
33 Zhai P-Y, Huang J-Q, Zhu L, Shi J-L, Zhu W, Zhang Q (2017) Calendering of free-standing electrode for lithium-sulfur batteries with high volumetric energy density. Carbon 111:493–501
34 Wu Z, Wang W, Wang Y, Chen C, Li K, Zhao G, Sun C, Chen W, Ni L, Diao G (2017) Three-dimensional graphene hollow spheres with high sulfur loading for high-performance lithium-sulfur batteries. Electrochim Acta 224:527–533
35 Song J, Xu T, Gordin ML, Zhu P, Lv D, Jiang YB, Chen Y, Duan Y, Wang D (2014) Nitrogen-doped mesoporous carbon promoted chemical adsorption of sulfur and fabrication of high-areal-capacity sulfur cathode with exceptional cycling stability for lithium-sulfur batteries. Adv Funct Mater 24:1243–1250
36 Qiu Y, Li W, Zhao W, Li G, Hou Y, Liu M, Zhou L, Ye F, Li H, Wei Z (2014) High-rate, ultralong cycle-life lithium/sulfur batteries enabled by nitrogen-doped graphene. Nano lett 14:4821–4827
37 Song J, Gordin ML, Xu T, Chen S, Yu Z, Sohn H, Lu J, Ren Y, Duan Y, Wang D (2015) Strong lithium polysulfide chemisorption on electroactive sites of nitrogen-doped carbon composites for high-performance lithium–sulfur battery cathodes. Angew Chem Int Ed 54:4325–4329